Spatial And Temporal Variability Of The Remotely Sensed Chlorophyll A Signal Associated With Rossby Waves In The South Atlantic Ocean

E. Gutknecht, I. Dadou, G. Charria, P. Cipollini, V. Garcon

JOURNAL OF GEOPHYSICAL RESEARCH, VOL. 115, C05004, doi:10.1029/2009JC005291, 2010

Spatial and temporal variability of the remotely sensed chlorophyll *a* signal associated with Rossby waves in the South Atlantic Ocean

E. Gutknecht,[1] I. Dadou,[1] G. Charria,[1,2] P. Cipollini,[2] and V. Garçon[1]

Received 23 January 2009; revised 22 October 2009; accepted 18 December 2009; published 4 May 2010.

[1] The present study focuses on the spatial and temporal variability of interactions between physics and biogeochemistry during the Rossby wave passage in the South Atlantic Ocean. The Rossby wave signature in sea level anomalies (SLA) and surface chlorophyll *a* concentration anomalies (CHLA) is analyzed using remotely sensed data from 1997 to 2006. Wavelengths between 400 and 1100 km, with westward propagating speeds up to 7.5 cm.s^{-1}, are observed. Using a theoretical model, three processes (meridional advection of surface chlorophyll *a* concentrations, uplifting of subsurface chlorophyll *a* maximum, and upwelling of nutrients) are likely to explain the chlorophyll *a* Rossby wave signature. A statistical assumption allows quantifying the relative importance of each process. Three zones are identified. The Subtropical Gyre is the only area where the contribution of the uplifting process reaches 20%. North and south of this gyre, the meridional advection process is responsible for an important part (around 60%) of the observed chlorophyll *a* signals. The temporal variability of this dominant process is studied using the phase relationships between CHLA and SLA and the surface meridional chlorophyll *a* gradient. A seasonal meridional shift (4°) is shown on both data sets on the area of negative meridional gradient. At 30°S–31°S, a clear seasonal cycle is observed in both data sets for the whole studied period, except in 2003 and 2004 where both data sets do not follow the usual seasonal cycle. These particular years can be related to anomalies in large scale atmospheric circulation over the South Atlantic Ocean.

Citation: Gutknecht, E., I. Dadou, G. Charria, P. Cipollini, and V. Garçon (2010), Spatial and temporal variability of the remotely sensed chlorophyll *a* signal associated with Rossby waves in the South Atlantic Ocean, *J. Geophys. Res.*, *115*, C05004, doi:10.1029/2009JC005291.

1. Introduction

[2] The South Atlantic Ocean plays an important role in the global oceanic circulation and climate variability. It connects the North Atlantic and Indian Oceans and its southern part communicates with the Pacific Ocean via the Antarctic Circumpolar Current. The South Atlantic Ocean exhibits a large frequency range of variability from intraseasonal to interannual up to multidecennial time scales, especially for the sea surface temperature (SST) [e.g., *Robertson et al.*, 2003; *Haarsma et al.*, 2003; *Grodsky and Carton*, 2006]. This variability is linked to fluctuations of the intensity and position of the South Subtropical Anticyclone in sea level pressure that affects the winds close to the ocean surface. Several hypotheses are proposed to explain the interannual variability in the South Atlantic Ocean: local coupled atmosphere/ocean interactions [e.g., *Venegas et al.*, 1997; *Sterl and Hazeleger*, 2003], atmospheric teleconnection with the Tropical Pacific [e.g., *Venegas et al.*, 1997; *Colberg et al.*, 2004; *Handoh et al.*, 2006], oceanic transport from the Indian Ocean [e.g., *Matano and Beier*, 2003], as well as Tropical Atlantic influences [e.g., *Grodsky and Carton*, 2006]. This variability affects the circulation of the South Atlantic Ocean.

[3] Rossby waves are also present in the South Atlantic Ocean and play a role in maintaining the midlatitude gyre and in the intensification of western boundary currents. These waves influence the South Atlantic Ocean circulation and variability. They were first theoretically studied in this basin by *Reason et al.* [1987]. They are mainly generated by fluctuations of winds on the eastern boundary of the basin (western African coast) as well as in the open ocean. The advance of satellite observations renewed the study of Rossby waves, especially with altimetry and ocean color data [*Chelton and Schlax*, 1996; *Machu et al.*, 1999; *Cipollini et al.*, 2001]. The South Atlantic Ocean exhibits the least intense signals of all basins in terms of wave amplitudes [*Polito and Liu*, 2003], but clear westward propagating signals can be identified on the longitude/time plots with the properties of first baroclinic mode of Rossby waves [*Charria et al.*, 2003]. However, *Chelton et al.* [2007] pointed out the fact that nonlinear eddies are expected to have phase speeds

[1]Laboratoire d'Etudes en Géophysique et Océanographie Spatiales, UMR 5566, UPS, CNES, CNRS, IRD, Toulouse, France.
[2]National Oceanography Centre, Southampton, UK.

0148-0227/10/2009JC005291

close to that of nondispersive Rossby waves, making it difficult to separate the two kind of signals.

[4] These Rossby waves have also a signature in satellite surface chlorophyll *a* concentrations [*Machu et al.*, 1999; *Cipollini et al.*, 2001; *Uz et al.*, 2001]. Horizontal (meridional advection of surface chlorophyll *a* concentrations) and vertical mechanisms (uplifting of subsurface chlorophyll *a* maximum and upwelling of nutrients) can explain this influence. Vertical processes associated with the passage of Rossby waves can increase/decrease the primary production [*Charria et al.*, 2008]. At basin scale, it may have an influence on the carbon cycle via the biological pump associated with the primary and subsequent export productions. These processes can potentially be modulated by the seasonal and interannual variability in the South Atlantic Ocean. In this paper, we focus our study on interactions between physics and biogeochemistry during the passage of Rossby waves and their spatial and temporal (seasonal and interannual) variability. We analyze the simultaneous satellite set of altimetry and ocean color data using spectral analyses. After a characterization of Rossby wave properties in the satellite data, we study the coupled processes which might explain this Rossby wave signal in surface chlorophyll *a* concentrations using a theoretical model [*Killworth et al.*, 2004; *Charria et al.*, 2006]. We then investigate the seasonal and interannual variability of the dominant process, and we attempt to interpret this process in the framework of the seasonal and interannual variability of the South Atlantic Ocean in the results and discussion section before concluding.

2. Data and Methods

2.1. Remotely Sensed Data Used

[5] As mentioned previously, two remotely sensed data sets are used in the studied area: sea level anomalies (SLA) derived from satellite altimeters and estimated surface chlorophyll *a* concentration anomalies (CHLA) from ocean color sensors.

2.1.1. Altimetry: Sea Level Anomalies

[6] Sea level anomaly (in cm) data from the DUACS (Data Unification and Altimeter Combination System) archive are developed by AVISO (Archivage, Validation et Interprétation des données des Satellites Océanographiques). An improved space/time objective analysis method combines TOPEX/Poseidon, ERS-1/2, JASON-1, GFO and ENVISAT data to obtain a merged sea level. This method takes into account long-wavelength errors (noise correlated on large scales) with a 1–2 cm mean error [*Le Traon et al.*, 1998]. SLA weekly products, obtained by subtracting the mean dynamic topography RIO05 [*Rio et al.*, 2005] from the sea surface height data, are projected on a regular spatial grid of 1/3° from October 1992 to August 2006 to obtain the mapped sea level anomaly products. To have the same temporal resolution as the monthly surface chlorophyll *a* concentrations (see below), SLA data are averaged monthly.

2.1.2. Ocean Color: Surface Chlorophyll *a* Concentrations

[7] Surface chlorophyll *a* concentrations (in $mgChl.m^{-3}$) are from the SeaWiFS (Sea-viewing Wide Field-of-view Sensor) ocean color sensor. We use monthly level 3 binned data products, processed (version 5.1) with the OC4v4 algorithm from *O'Reilly et al.* [1998]. Data are processed by the NASA Goddard Space Flight Center and distributed by the DAAC (Distributed Active Archive Center) [*McClain et al.*, 1998]. Monthly products are projected on a regular spatial grid of 9 km and cover a period of almost 9 years from the start of the SeaWiFS mission (September 1997) to August 2006. The predicted error on the 1 km SeaWiFS estimates of surface chlorophyll *a* concentrations is 35% [*McClain et al.*, 1998]. The accuracy of 9 km gridded data is comparable or better. Monthly data are regridded onto a regular spatial grid of 1/3° to have the same spatial resolution as SLA, sufficient to detect large scale propagating signals.

[8] Chlorophyll *a* concentrations in the ocean tend to be lognormally distributed [*Campbell*, 1995; *Pottier et al.*, 2006]. Therefore, we take the decimal logarithm of surface chlorophyll *a* concentrations. Gaps in the data, mainly due to the presence of clouds, are filled with a linear interpolation necessary for the application of the spectral analysis and filters described below. These gaps have a mean value of 51 km ± 37 km between 18°S and 45°S, or 13% ± 9% of the minimum wavelength (400 km) of the Rossby waves studied.

2.1.3. Studied Domain

[9] The analyzed area between 18°S and 45°S varies in longitude (from 39°W to 6°E for the maximum zonal extension). Coastal areas as well as regions north of 18°S and south of 45°S are masked out. Indeed, regions with high surface chlorophyll *a* concentrations on the borders of data series (for example, the Benguela Upwelling and the Brazil-Malvinas Confluence Zone) may induce strong edge effects in the spectral analysis and generate important spectral coefficients which may mask the weaker signals linked to Rossby waves. Moreover, closer to the equator, the equatorial region has dense cloud coverage. Southward of 40°S, the dynamics are complicated by the strong advection of the Antarctic Circumpolar Current inducing eastward propagating features [*Hughes*, 1995]. Furthermore, the observation of Rossby waves from ocean color data becomes very difficult south of 45°S because of persistent winter cloud cover. Therefore, we choose 45°S as the southern boundary of the studied area.

[10] Since the eastern boundary of the South Atlantic Ocean is removed from our studied domain, the beta refraction effect toward the equator of low latitude baroclinic Rossby wave packets due to the strong dependence of the zonal group velocity *Cg* on latitude [see *Schopf*, 1981; *Pierini*, 2005, 2006] cannot be seen.

2.2. Signal Analysis Methodology and Westward Propagations

[11] In the present work, the wavelet analysis (WA) as in the work of *Charria et al.* [2006] is used. This spectral analysis, based on the Wavelet Transform (WT), allows finding the dominant frequencies of the signal and their locations in space and/or time. For a one-dimensional WA, the WT uses a family of functions, called *wavelets*, based on two parameters: the translation and the dilatation [*Kumar and Foufoula-Georgiou*, 1994]. We are using the 1-D continuous WT defined as a convolution of a discrete sequence and a translated and dilated *wavelet* [*Torrence and Compo*, 1998]. We adopt the *Morlet wavelet*, a modulated Gaussian plane

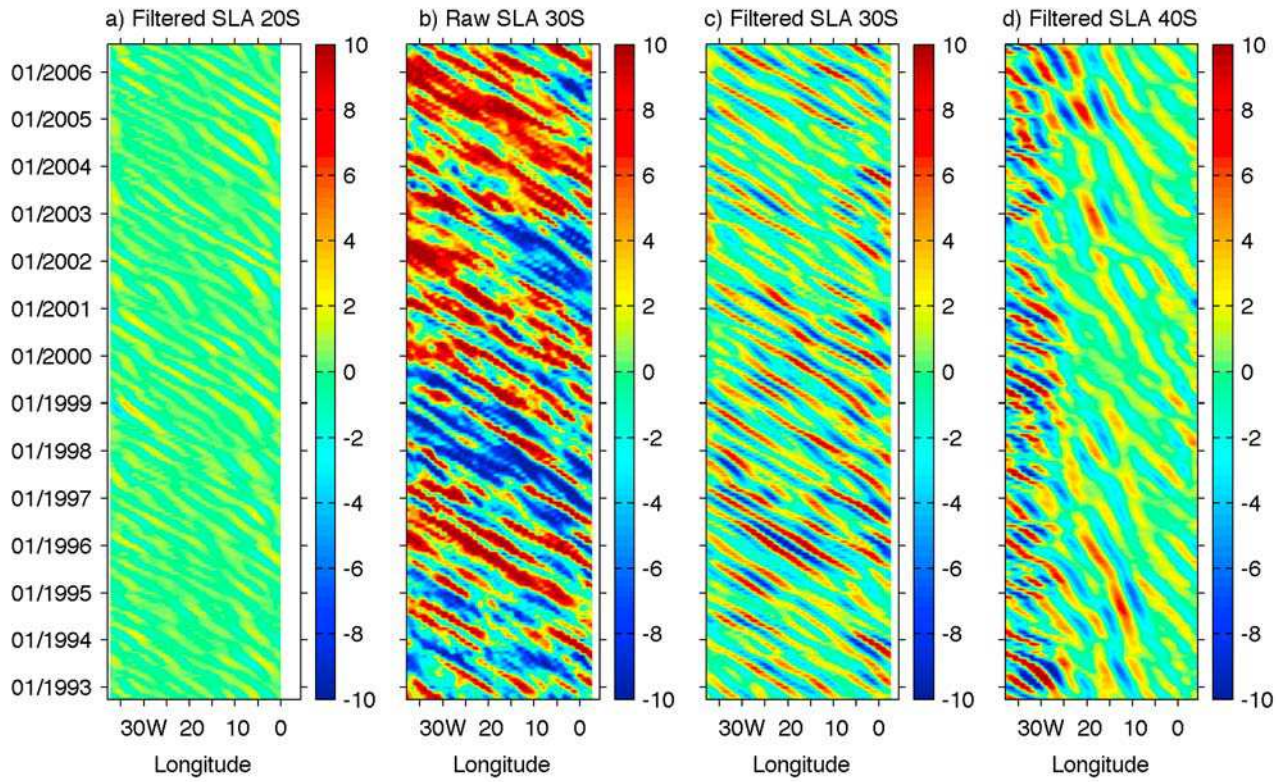

Figure 1. Longitude/time diagrams of SLA (cm) at (a) 20°S, (c) 30°S, and (d) 40°S for filtered data and (b) 30°S for raw data. Signals are reconstructed for wavelengths between 400 and 1100 km, after removing eastward propagating and stationary features.

wave suitable for the analysis of waves in Geophysics. This method is spatially applied, for each latitude (between 18°S and 45°S) and each time step, to study wavelengths of the dominant propagating signals in altimetry and ocean color data sets. The cross-wavelet analysis (CWA [see *Torrence and Webster*, 1999]) is then applied to both data sets, which allows for the quantification of the coherency and phase relationships (or phase differences) between these two data sets. We focus here our investigation on the possible phase relationships between CHLA and SLA.

[12] The first baroclinic mode of Rossby waves corresponds to westward propagating signals, which can be nondominant in SLA and/or surface chlorophyll *a* concentrations as compared to other processes such as the seasonal cycle or nonlinear eddies. To clearly identify these propagations, a preprocessing is necessary. In our case, we choose to apply two spectral filters. First, the eastward propagating (corresponding to those spectral components for which wave number and frequency have the same sign, i.e., those in the first and third quadrants) and stationary features (those with zero frequency, i.e., on the wave number axis) are removed using a 2-D (longitude/time) Fourier analysis for each latitude. By removing stationary features, zonal mean values are removed from SLA and surface chlorophyll *a* concentrations. Surface chlorophyll *a* concentration anomalies (CHLA) are then obtained. Components with zero wave number are also removed [*Killworth et al.*, 2004]. In a second step, CHLA and SLA signals are reconstructed for wavelengths included between 400 km and 1100 km, using a 1-D spatial WA performed for each latitude and time step. The choice of this wavelength range allows filtering out part of the mesoscale signals (for nonlinear eddies with diameters lower than 200 km). This wavelength interval was emphasized by a preliminary WA carried out on the SLA data after removing only the stationary and eastward propagating features (see section 3.1). A filtered data set is then obtained and westward propagations are clearly observed in longitude/time diagrams of SLA as compared to the unfiltered data (see the example at 30°S, Figures 1b and 1c).

[13] We tested our filtering procedure to ensure that removal of eddies was performed efficiently using an idealized 3-D model (M. Thomas, personal communication, 2009). This model simulates statistically realistic Gaussian eddies based on *Chelton et al.* [2007], a set of idealized sinusoidal waves, and a final model field (or mesoscale field) containing both eddy and Rossby wave components. The filtering procedure is then applied on the mesoscale field in order to split the signal into eddy component and linear Rossby wavefields, and demonstrate the efficiency of the filter to remove a large fraction of eddies. The filtering procedure successfully removes a large fraction of simulated eddies (not shown) and can be applied to real data with confidence. However, some of them subsist after filtering, west of 25°W southward of 40°S because of the high mesoscale activity associated with the Brazil-Malvinas Confluence Zone.

[14] Propagation speeds (the phase velocities of Rossby waves) are estimated using the Radon transform (RT) [*Deans*, 1983]. This method, frequently used to estimate phase speeds in oceanic data sets [e.g., *Challenor et al.*,

2001; *Maharaj et al.*, 2005; *Cipollini et al.*, 2006; *Charria et al.*, 2006], is applied on 2-D filtered SLA longitude/time diagrams.

2.3. Modeling of the Physical/Biological Coupled Processes

2.3.1. Different Mechanisms and Associated Phase Relationships Between CHLA and SLA

[15] To investigate the different physical/biogeochemical coupled processes involved in the signature of Rossby waves in CHLA, *Killworth et al.* [2004] modeled each one of the three different mechanisms responsible for the coupling, and predicted the resulting phase relationships between CHLA and SLA.

2.3.1.1. Horizontal Mechanism: Meridional Advection of Surface Chlorophyll *a* Concentrations

[16] Westward propagating Rossby waves generate periodic sea surface height anomalies alternatively positive and negative (crests and troughs, respectively) [*Killworth et al.*, 2004]. Owing to geostrophic balance, there are meridional velocities of alternate signs in the SLA zonal gradients on the flanks of the waves. A field of westward propagating waves superimposed on a background meridional chlorophyll *a* gradient (north-south) will therefore distort the front of chlorophyll *a* concentrations because of those geostrophic velocities, resulting into an alternation of positive and negative anomalies in the chlorophyll *a* field that propagate westward with the waves.

[17] For this horizontal mechanism, the theoretical spatial phase relationships depend on the sign of the meridional chlorophyll *a* gradient and on the studied hemisphere. In the South Atlantic Ocean, the following three situations can be observed [see *Killworth et al.*, 2004, Figure 8] (see section 2.3.2):

[18] 1. North of the Subtropical Gyre northern boundary, a positive meridional chlorophyll *a* gradient ($\partial[Chl]/\partial y > 0$) gives spatial phase relationships between $-\pi/2$ and 0. The northern boundary of the gyre is leaning northwest/southeast, situated at about 15°S in the western part of the basin and at about 30°S in the eastern part.

[19] 2. In the Subtropical Gyre, between the northern boundary and about 39°S, the negative meridional chlorophyll *a* gradient ($\partial[Chl]/\partial y < 0$) gives spatial phase relationships between $\pi/2$ and π. The gradient is very weak in the oligotrophic gyre, between the northern boundary and about 30°S. It becomes strongly negative in the southern part of the gyre until the Subtropical Front, between about 30°S and 39°S.

[20] 3. Between about 39°S and 45°S, a positive meridional chlorophyll *a* gradient ($\partial[Chl]/\partial y > 0$) gives spatial phase relationships between $-\pi/2$ and 0.

2.3.1.2. Vertical Mechanism 1: Uplifting of Subsurface Chlorophyll *a* Maximum

[21] Several oceanic regions have a subsurface chlorophyll *a* maximum located within 10 m depth. A propagating wave generates isopycnal vertical movements. Uplift of isopycnals subsequent to the passage of Rossby waves allows an uplifting of phytoplankton cells that can be remotely detected [*Cipollini et al.*, 2001; *Charria et al.*, 2003] and thus can generate an anomaly of surface chlorophyll *a* concentrations.

2.3.1.3. Vertical Mechanism 2: Upwelling of Nutrients

[22] Upwelling associated with Rossby waves could bring additional nutrients into the euphotic layer [*Cipollini et al.*, 2001; *Killworth et al.*, 2004]. Indeed, Rossby waves pump nutrients upward during their westward propagation across the oceanic basin, the so-called Rototiller effect [*Siegel*, 2001]. Following the structure of the wave, these new nutrients in the euphotic zone would be assimilated and converted into chlorophyll *a* by phytoplankton. These wavelike structures, propagating at the same speed as Rossby waves, could be detected by an ocean color sensor.

[23] For the two last vertical coupled processes, it can be theoretically demonstrated that the predicted spatial phase relationships are between $\pi/2$ and π [*Killworth et al.*, 2004] in the case of a spatial analysis (see section 2.3.2).

2.3.2. Relative Contribution of the Different Processes

[24] A more quantitative approach, based on amplitude ratios and phase relationships between CHLA and SLA, can be adopted to identify the relative contribution of the processes that can explain the chlorophyll *a* signal of Rossby waves.

[25] The theoretical model from *Killworth et al.* [2004] describes the evolution of a tracer (C) advected by a purely westward propagating Rossby wave. Based on this advection/diffusion equation, a complex expression of the ratio between the amplitude of the tracer signal (C_A) and the sea surface height (η_A), detailed enough to express the various possible combinations of mechanisms, is obtained

$$\frac{C_A}{\eta_A} = \left|\frac{C_A}{\eta_A}\right| e^{i\varphi} = \frac{g}{f}\,\frac{\left(\overline{C}_{0y} - \beta\Delta C/f\right)}{\left(c - \overline{u}_0 + ic/\omega\tau\right)}, \tag{1}$$

where φ is the phase difference ($\varphi = (phase(C_A) - phase(\eta_A))$), g is the acceleration due to gravity, c the negative phase speed of the wave (because of westward propagation) determined from the wave number $k = \omega/c$ (negative), ω the wave frequency (positive). $\overline{u}_0$ is the zonal mean current, f the Coriolis parameter and $\beta = df/dy$ the northward gradient of the Coriolis parameter. The subscript ($_0$) represents the surface values. $\overline{C}_{0y}$ is the horizontal meridional tracer gradient (estimated from SeaWiFS ocean color data averaged between 1998 and 2001). Limiting nutrients are assumed to be nitrates, which is a reasonable assumption over the South Atlantic Ocean [*Killworth et al.*, 2004], north of 50°S. $\Delta C \equiv \overline{C}(z = 0) - \overline{C}(z = -h)$ with $h = 50$ m for nutrients (chosen value for the mixed layer depth using the nitrate climatology of *Louanchi and Najjar* [2001]) and $h = 10$ m for chlorophyll *a* (for the reasons outlined by *Killworth et al.* [2004]). τ is the relaxation time, i.e., the response time of the system to come back at a steady state after a perturbation, here taken to be 20 days. In equation (1), the mixing term is simply parameterized as the relaxation time τ after a perturbation. This time scale represents the necessary time of the whole biogeochemical processes to eliminate a nutrient anomaly. All chosen values for the different parameters are taken from *Killworth et al.* [2004].

[26] Equation (1) allows the modeling of the three different mechanisms, and can be rewritten as

$$\frac{C_A}{\eta_A} = \left|\frac{C_A}{\eta_A}\right| e^{i\varphi} = |A|\, e^{i[1-\mathrm{sign}(A)]\frac{\pi}{2}}\,\frac{(c - \overline{u}_0 - ic/(\omega\tau))}{(c - \overline{u}_0)^2 + (c/\omega\tau)^2}. \tag{2}$$

With

$$A = \left(\frac{g\overline{C}_{0y}}{f} - \frac{g\beta\Delta C}{f^2}\right). \quad (3)$$

The *sign* function returns the sign of the above quantity called A. So if $A > 0$: $sign(A) = +1$, and if $A < 0$: $sign(A) = -1$.

[27] Defining Φ such that

$$\cos\Phi = \frac{(c - \overline{u}_0)}{\sqrt{(c - \overline{u}_0)^2 + (c/\omega\tau)^2}} \quad (4)$$

$$\sin\Phi = \frac{(-c/(\omega\tau))}{\sqrt{(c - \overline{u}_0)^2 + (c/\omega\tau)^2}}. \quad (5)$$

We have then

$$\varphi = \left((1 - \mathrm{sign}(A)\frac{\pi}{2} + \Phi\right). \quad (6)$$

As shown by *Killworth et al.* [2004], the different cases can be summarized as follows:

$$\text{If } \omega\tau \ll 1 \quad \text{then} \quad \varphi = (2 - \mathrm{sign}(A))\frac{\pi}{2}, \quad (7)$$

$$\text{If } \omega\tau \gg 1 \quad \text{then} \quad \varphi = (3 - \mathrm{sign}(A))\frac{\pi}{2}, \quad (8)$$

$$\text{And if } \Delta C = 0 \quad \text{then} \quad A = \left(\frac{g\overline{C}_{0y}}{f}\right), \quad (9)$$

$$\text{And if } \overline{C}_{0y} = 0 \quad \text{then} \quad A = \left(-\frac{g\beta\Delta C}{f^2}\right). \quad (10)$$

The horizontal advection case is computed by taking C as surface chlorophyll a concentrations and removing the effect of the vertical advection ($\Delta C = 0$). The vertical advection processes are simulated removing the tracers horizontal gradients ($\overline{C}_{0y} = 0$), then taking C to represent either surface chlorophyll a concentrations to solve the vertical advection of chlorophyll a (ΔC calculated using the climatology of *Conkright et al.* [1998]), or nutrient concentrations (then converted to chlorophyll a assuming a constant Chl:N ratio $\Delta C = 1.59\Delta N$ estimated using the climatology of *Louanchi and Najjar* [2001]) for the upwelling case. Using these different formulations, amplitude ratios ($|C_A/\eta_A|$) and phase relationships (φ) from each process can be analyzed.

[28] So in the South Atlantic Ocean, we get for the following different cases: (1) if $\Delta C = 0$, the horizontal process dominates and $\varphi \in [\pi/2\ \pi]$ for negative meridional chlorophyll gradient and $\varphi \in [-\pi/2\ 0]$ for positive meridional chlorophyll gradient and (2) if $\overline{C}_{0y} = 0$, the vertical processes dominate and $\varphi \in [\pi/2\ \pi]$.

[29] To study the relative contribution of the three different coupled processes, we added a statistical assumption that allows a quantitative decomposition of the contributions by the different processes, by combining together modeled and observed amplitudes ratios and phase relationships [*Charria et al.*, 2006].

[30] We assumed that the observed amplitude ratios and phases could be written as a linear combination of the three modeled processes. So, the following equation can be built:

$$\left|\frac{C_A}{\eta_A}\right|_{obs} e^{i\varphi_{obs}} = z_\alpha \left|\frac{C_A}{\eta_A}\right|_{hadv} e^{i(\varphi_{hadv})} + z_\beta \left|\frac{C_A}{\eta_A}\right|_{upl} e^{i(\varphi_{upl})} + z_\gamma \left|\frac{C_A}{\eta_A}\right|_{upw} e^{i(\varphi_{upw})}, \quad (11)$$

where z_α, z_β and z_γ are three unknown parameters associated with the different modeled complex amplitudes: horizontal advection (*hadv*), uplifting of chlorophyll a (*upl*) and upwelling of nitrates (*upw*). These parameters are complex (for example, $z_\alpha = \alpha\ \exp(i\varphi_\alpha)$) in order to encompass both amplitude and phase errors in the model.

[31] The system (11) has six unknown parameters in two equations (real and imaginary parts) and then an infinite number of solutions. Among the different possible solutions, we select the one that gives the smallest value for the following cost function:

$$\Psi = \sqrt{|z_\alpha - 1|^2 + |z_\beta - 1|^2 + |z_\gamma - 1|^2}. \quad (12)$$

The cost function Ψ describes the distance, in parameters' space, between the three complex parameters (a point with coordinates (z_α, z_β, z_γ)) and number one (the point (1,1,1)), based on the idea that if the process modeling is correct then all the three coefficients would be equal to unity. In other words, z_α, z_β or z_γ equal one represents a total contribution by the corresponding process, exactly as modeled (with exactly modeled amplitude and phase), to reproduce the observations. Solving (11) by minimizing Ψ allows extracting a set of parameters to reproduce the observed amplitude ratios and phase relationships. The relative contribution (P) of the three different processes involved in the signature of Rossby waves in the South Atlantic Ocean is then computed using the following equation:

$$P_j = 100 \times \frac{z_j |C_A/\eta_A|_j}{z_\alpha |C_A/\eta_A|_\alpha + z_\beta |C_A/\eta_A|_\beta + z_\gamma |C_A/\eta_A|_\gamma}, \quad (13)$$

where $j = \alpha,\ \beta,\ \gamma$.

3. Results and Discussion

3.1. Rossby Wave Signature in SLA and CHLA in the South Atlantic Ocean

3.1.1. Westward Propagations Observed in SLA

[32] Westward propagating signals, previously identified by several authors as the first baroclinic mode of Rossby waves from their dynamical features (for a review, see *Fu and Chelton* [2001]), are clearly observed in longitude/time plots of filtered SLA at all latitudes studied between 18°S and 45°S (see examples at 20°S, 30°S and 40°S on Figure 1). At 20°S and 30°S, propagations are distinct and keep roughly the same amplitude (3 cm and 10 cm, respectively) across the basin. At 30°S, waves do not exhibit any disturbance, probably due to a waveguide at 30.5°S [*Polito and Liu*, 2003]. At 40°S, the high mesoscale activity

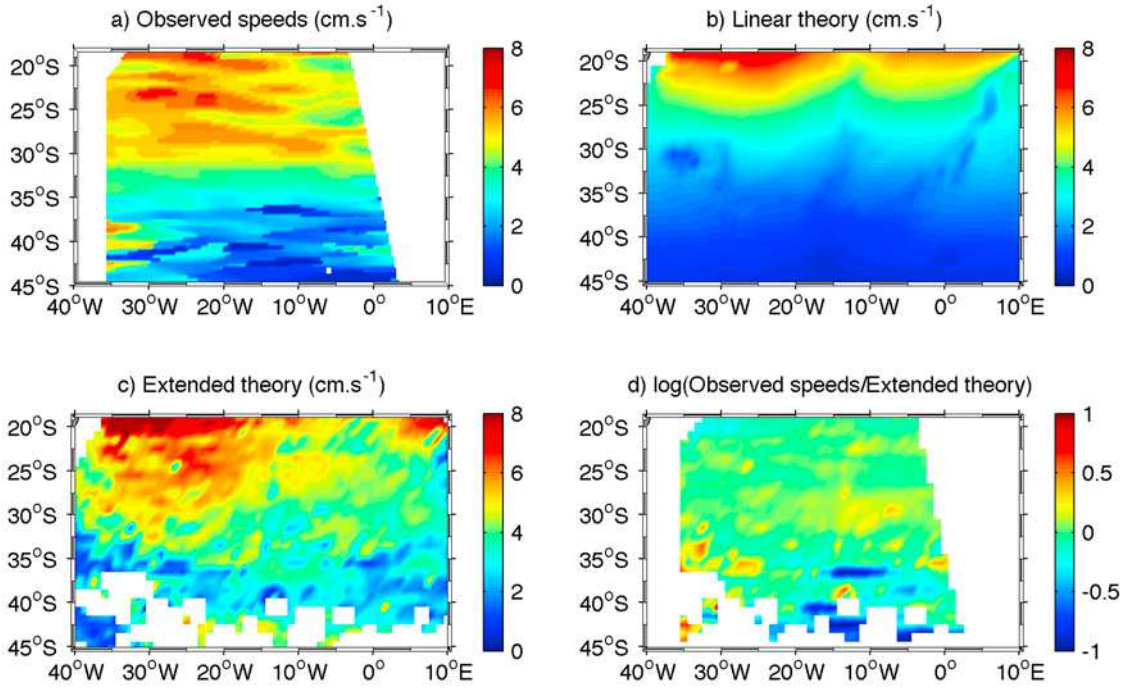

Figure 2. Propagation speeds (cm.s^{-1}, positive westward) corresponding to (a) the filtered SLA data, (b) the linear theory, and (c) the extended theory. (d) Logarithm of the ratio between speeds deduced from the observations and the extended theory. In Figures 2a and 2d, data close to the coasts are omitted due to strong zonal chlorophyll *a* gradients which introduce edge effects in the WA.

(i.e., eddies, fronts, meanders) associated with the Brazil-Malvinas Confluence Zone and the wave/current interactions in this region amplify the propagations west of 20°W.

3.1.2. Zonal Phase Velocities

[33] Observed zonal westward propagation velocities associated with Rossby waves increase from less than 1 cm.s^{-1} in some areas close to 45°S to more than 7.5 cm.s^{-1} at 18°S (Figure 2a), in agreement with *Polito and Liu* [2003]. Such a dependence on latitude is expected from both the linear theory for the first baroclinic mode of Rossby waves (Figure 2b) and its recent extension (Figure 2c) [*Killworth and Blundell*, 2003a, 2003b]. The observed westward increase of the speeds (Figure 2a) is well described by this extended theory (Figure 2c) because it takes into account the mean baroclinic currents, the stratification and the oceanic topography. The ratio between the observed phase speeds and the velocities of the extended theory (Figure 2d) exhibits a good agreement in most of the locations, despite some differences in a few localized areas. The presence of slower waves than the theory south of 40°S (Figure 2d) is probably due to the Doppler shift induced by the barotropic mean current (northern branch of the Antarctic Circumpolar Current) [*Hughes*, 1995], which is not considered in the extended theory.

3.1.3. Wavelengths

[34] A preliminary 1-D WA was performed on the SLA data after removing only the stationary and eastward propagating features to extract wavelengths for the maximum wavelet coefficients at each latitude and each month (see section 2.2). The results highlight a strong latitudinal variability of the signal, with an equatorward increase of the wavelengths from about 455 km at 45°S to 1050 km at 18°S on temporal mean. This wavelength range corresponds to the wavelength range associated with the cross-spectral peak found by *Killworth et al.* [2004] in the South Atlantic Ocean (between 500 km and 1000 km [see *Killworth et al.*, 2004, Figure 6d]), and in other oceans for this latitude range.

3.1.4. Westward Propagations Observed in CHLA

[35] On Figure 3, three examples of longitude/time diagrams in $\log_{10}$(CHLA) computed with the same methodological approach as for the SLA are shown. Westward propagating features observed at 20°S, 30°S and 40°S are very similar to Rossby wave signals detected in SLA with wavelengths between 400 km and 1100 km. This confirms the findings by *Cipollini et al.* [2001], *Uz et al.* [2001], and *Charria et al.* [2003, 2006] that Rossby waves have a signature in ocean color data, although filtering is often required to highlight this signature, otherwise hidden by other sources of variability. Thus, westward propagating features (Rossby waves and/or nonlinear eddies, especially in the western boundary) are a nonnegligible source of chlorophyll *a* variability in the South Atlantic Ocean. Nevertheless, many propagating features faster than Rossby waves (i.e., instabilities, meanders) are also observed at 40°S west of 20°W in the Confluence Zone (Figure 3c).

3.2. Coupled Physical/Biogeochemical Processes Involved: A Dominant Process?

[36] As presented before (see section 2.3.1), three physical/biogeochemical coupled processes are likely to explain the signature of Rossby waves in CHLA: the meridional advection of surface chlorophyll *a* concentrations, the uplifting of subsurface chlorophyll *a* maximum and the upwelling

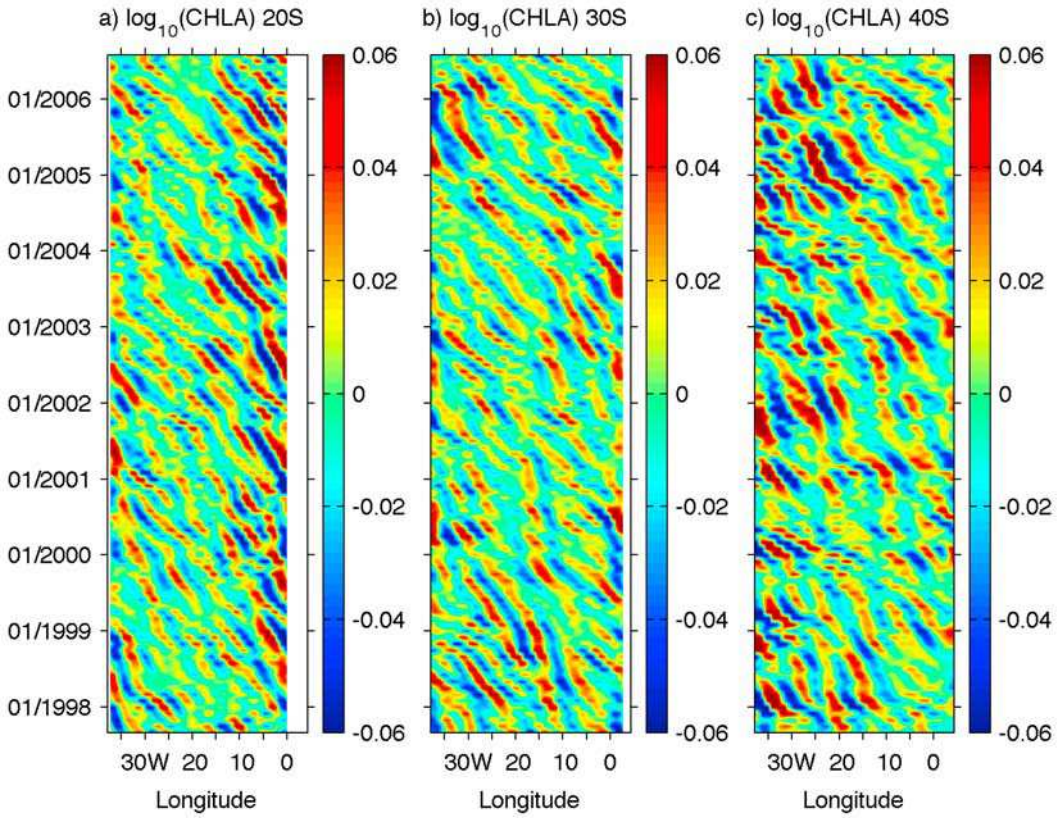

Figure 3. Longitude/time diagrams of $\log_{10}$(CHLA) ($\log_{10}$(mgChl.m^{-3})) at (a) 20°S, (b) 30°S, and (c) 40°S. Signals are reconstructed for wavelengths between 400 and 1100 km, after removing eastward propagating and stationary features.

of nutrients. In this section, we address the question of which mechanism dominates in the South Atlantic Ocean, following the methodology developed by *Charria et al.* [2006], which is an extension of the approach suggested by *Killworth et al.* [2004] (see section 2.3.2).

3.2.1. Spatial Variability of Phase Relationships Between CHLA and SLA

[37] We analyze the phase relationships between the filtered CHLA and SLA signals using a CWA. Wavelet coherency and phase relationships (φ = *phase*(*CHLA*) − *phase*(*SLA*)) are computed for each latitude from 18°S to 45°S and for each month from September 1997 up to August 2006. From each local wavelet power spectrum, the phase for components between 400 km and 1100 km (within the cone of influence, to exclude the edge effects [see *Torrence and Compo*, 1998]), having a coherency above 0.75 [*Charria et al.*, 2006], is then extracted. For the whole time series, the percentage of cross-wavelet coefficients having a coherency above 0.75 is approximately the same for each month and each year (between 61.3% and 66.5% with a mean value of 63.3%; Figure 4a). The largest number of strong coherencies between CHLA and SLA is reached in the southern part of the Subtropical Gyre (between 32°S and 38°S), with 70% to 84% of values above 0.75 in temporal average (Figure 4b).

[38] The temporal average of phase relationships is performed by summing the wavelet coefficients in the complex space. The percentage of data contributing to the estimate of the phase differences is the most important (>80%) between 32°S and 38°S. It stays above 50% on the rest of the domain, except on the borders (Figure 4d). Figure 5a presents the phase relationships between CHLA and SLA signals using the CWA. In order to compare our results with those obtained by *Killworth et al.* [2004] using the 2-D Fourier cross-spectral analysis (Figure 5b), we show the results from the 1998–2001 period only (Figure 5a). However, the phase differences obtained for the whole time series using the CWA (not shown) are very similar to those from the 1998–2001 period only. Due to the propagation being westward, the spatial phase map on Figure 5b has opposite sign as compared to the temporal phase map on Figure 6h in the work of *Killworth et al.* [2004]. The phase relationships by both methods (Figures 5a and 5b) appear to be in good agreement and are correlated with the meridional chlorophyll *a* gradient [see *Killworth et al.*, 2004, Figure 8].

[39] In areas of strong positive meridional chlorophyll *a* gradient, north of the Subtropical Gyre northern boundary (see white solid line on Figure 5b) and south of 39°S (see white dotted line on Figure 5b), phases are mainly between $-\pi/2$ and 0 (Figure 5a). However, phases between $-\pi$ and $\pi/2$ are also observed in the area north of the Subtropical Gyre northern boundary, and the area south of 39°S also contains phases between 0 and $\pi/2$ (especially south of 42°S). Based on phase relationships, meridional advection of surface chlorophyll *a* concentrations could explain the Rossby wave

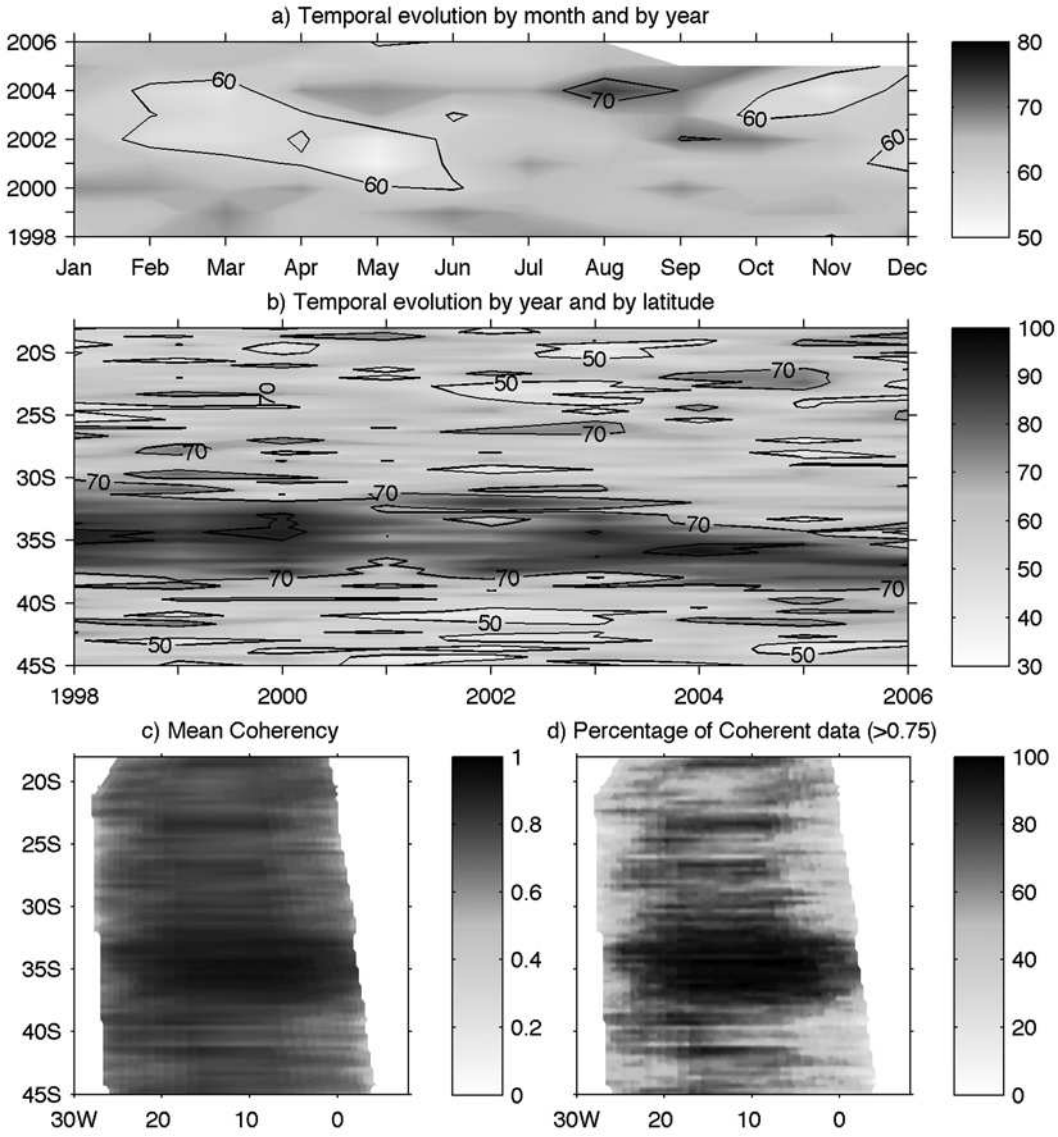

Figure 4. Ratio of extracted data as compared to the number of data used for the CWA: (a) temporal evolution of the percentage (%) by month and by year, (b) temporal evolution of the percentage (%) by year and by latitude, (c) temporal average (from 1998 to 2001) of all coherencies above 0, and (d) percentage (%) of data having a coherency above 0.75 over 4 years (1998 – 2001).

signals in ocean color in most of those locations where observed phases are between $-\pi/2$ and 0 (see section 2.3.1).

[40] Between 39°S and the Subtropical Gyre northern boundary, the phase relationships are mainly between $\pi/2$ and π (Figure 5a) ($\varphi = -\pi$ is equivalent to $\varphi = \pi$), especially between 30°S and 39°S where coherencies deduced from the CWA are the most significant (with values which can be higher than 0.95; not shown). In this area of negative meridional chlorophyll *a* gradient, such a range of phases can arise from both vertical and horizontal processes (see section 2.3.1). North of 30°S, some locations exhibit phase relationships between $-\pi/2$ and $\pi/2$ where the meridional chlorophyll *a* gradient is weakly negative in this oligotrophic zone. So between 39°S and the Subtropical Gyre northern boundary, the simple examination of the phase relationships does not allow a straightforward determination of a dominant process. Further analysis, described below, is needed to assess the relative contribution of the different processes.

3.2.2. Relative Contribution of the Different Processes: Importance of the Chlorophyll *a* Horizontal Advection

[41] The results of the time independent theoretical model (see section 2.3.2), which computes amplitude ratios ($|C_A/\eta_A|$) and phase relationships (φ) for each process, are compared to the observed amplitude ratios and phase relationships for the whole area studied. We are using the observations from *Killworth et al.* [2004] (see Figure 5b), as these already represent averages over the same time series (1998–2001). The method from *Charria et al.* [2006] (see section 2.3.2) is then applied at all latitudes from 18°S to 45°S in order to identify the relative contribution of the

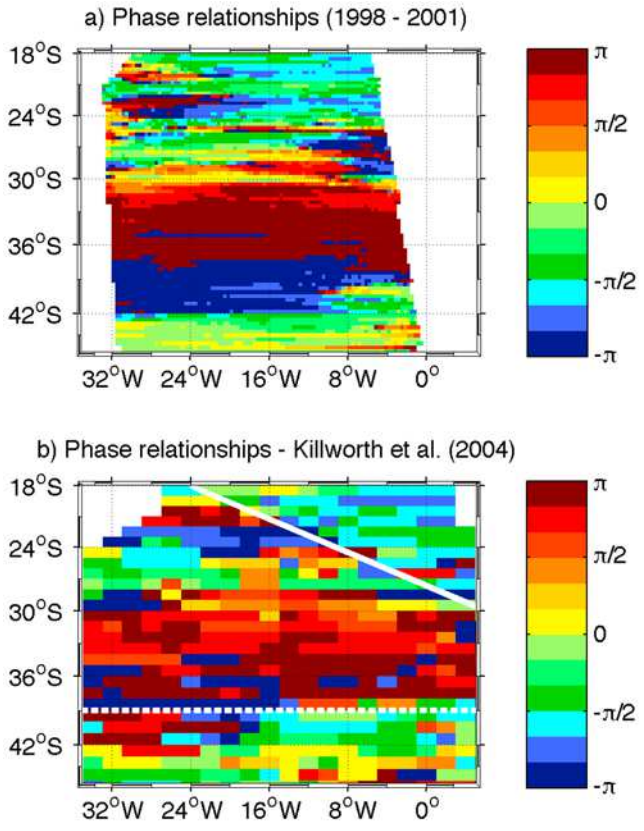

Figure 5. Phase relationships between SLA and CHLA ($phase(CHLA) - phase(SLA)$). (a) Spatial phase relationships are computed using the CWA. Phases for data having a maximum coherency > 0.75 are extracted from each local wavelet power spectrum in the cone of influence for wavelengths between 400 and 1100 km. If there is more than one maximum coherency in the spectral domain, the point in the physical space is excluded to retain only unambiguous phases. (b) Spatial phase relationships found by *Killworth et al.* [2004] over the time series from 1998 to 2001, computed using the Fourier cross-spectral analysis. The white solid line and the white dotted line represent the Subtropical Gyre northern limit and the 39°S limit, respectively (see section 3.2.2).

three processes explaining the influence of Rossby waves on surface chlorophyll *a* concentrations in the South Atlantic Ocean and to resolve any ambiguity whenever possible.

[42] This basin scale method allows distinguishing three different subdomains (limits plotted on Figure 5b) previously suggested by the meridional chlorophyll *a* gradient and the phase relationships deduced from remotely sensed data (see section 3.2.1). Figure 6 shows the results on ternary diagrams for the following three distinct subdomains:

[43] 1. North of the Subtropical Gyre northern boundary (oriented northwest/southeast; the white solid line on Figure 5b), the meridional advection of surface chlorophyll *a* concentrations is the dominant process, with a mean relative contribution of 63.2%. The mean relative contribution is 33.5% for the upwelling of nitrates, and 3.3% for the uplifting of subsurface chlorophyll *a* concentrations.

[44] 2. Between the northern boundary of the Subtropical Gyre and 39°S, the horizontal advection process contributes to 48.5%, the uplifting of subsurface chlorophyll *a* concentrations to 20.5%, the upwelling of nitrates to 31%. The contribution of the uplifting process needs to be highlighted because it is not observed in the other two areas. *Charria et*

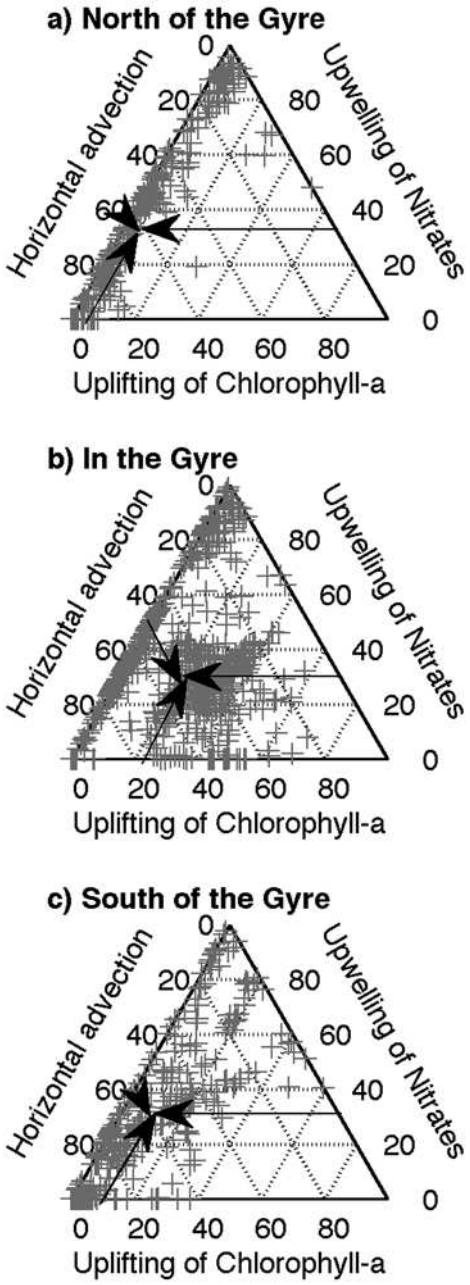

Figure 6. Relative contribution (in %) of the three assumed processes which can explain the surface chlorophyll *a* signature of Rossby waves: meridional advection of surface chlorophyll *a* concentrations, upwelling of nitrates in the euphotic zone and uplifting of the subsurface chlorophyll *a* maximum. Crosses represent all model grid points (a) north of the Subtropical Gyre northern boundary, (b) between the northern boundary of the Subtropical Gyre and 39°S, and (c) south of 39°S for a domain between 18°S and 45°S.

al. [2003] using the same data set [*Conkright et al.*, 1998] as *Killworth et al.* [2004] as well as a radiative transfer model, suggest that the vertical chlorophyll *a* advection could explain part of the observed signal in the Subtropical Convergence Zone, where the vertical chlorophyll *a* gradient is high.

[45] 3. South of 39°S, the horizontal process is the main contributor (58.8%) with most of the values higher than 50%. Uplifting of subsurface chlorophyll *a* concentrations contributes to 9.7% and upwelling of nitrates to 31.5%.

[46] The meridional advection of surface chlorophyll *a* concentrations by Rossby waves is the dominant process, responsible of an important part of the observed signals in the chlorophyll *a* data. Previous studies (*Quartly et al.*'s [2003] study of the South Indian Ocean and *Killworth et al.*'s [2004] study of the global ocean) also showed that the primary mechanism explaining a Rossby wave signal in ocean color appears to be the meridional advection of water across a strong chlorophyll *a* gradient. The significant contribution of the purely vertical advection of subsurface chlorophyll *a* concentrations is restricted to the Subtropical Gyre. *Charria et al.* [2003] and *Killworth et al.* [2004] showed that in the Subtropical Convergence Zone, a reasonably small upwelling velocity acting against a strong vertical chlorophyll *a* gradient over the top 10 m [see *Killworth et al.*, 2004, Figure 10h] can produce a strong surface signal. The process of upwelling of nutrients represents almost the same contribution in the entire studied area (~32%). This process could potentially have an influence on the primary production and, thus play a role in the carbon cycle through "the biological pump." Indeed, a study in the North Atlantic Ocean showed local increases/decreases of the primary production of about ± 20% associated with Rossby wave propagations [*Charria et al.*, 2008] in several locations. Compared to the North Atlantic Ocean using the same method [*Charria et al.*, 2006], the situation is different in the South Atlantic Ocean mainly due to the presence of the Subtropical Convergence Zone, which generates an important front in surface chlorophyll *a* concentrations.

[47] Some caveats have to be made on these results. Rossby waves represent a major process in the ocean, which can be studied using satellite observations. However, the formal identification of Rossby waves remains tricky. The first moderation comes from the existence of nonlinear eddies, which, when observed by surface longitude/time diagrams, have spectral characteristics similar to Rossby waves [*Chelton et al.*, 2007]. *Chelton et al.* [2007] suggested that more than 50% of the variability over much of the World Ocean was explained by nonlinear eddies with amplitude between 5 cm and 25 cm and diameter between 100 and 200 km. These nonlinear eddies propagate almost westward at approximately the phase speed of non dispersive baroclinic Rossby waves. From 25° to the equator, eddy speeds are slower than zonal phase speeds of non dispersive baroclinic Rossby waves predicted by the classical theory. Elsewhere, eddy speeds are very similar to the westward phase speeds of classical Rossby waves. Thus, in our study, westward propagations observed between 25°S and 45°S may correspond both to Rossby waves and nonlinear eddies, and eddies should be important particularly in the Subtropical Convergence Zone due to the strong mesoscale activity there [*Longhurst*, 1998]. However, as the data used in our study are filtered for wavelengths below 400 km, we therefore remove a large fraction of these nonlinear eddies between 100 and 200 km diameter, except in the region of western boundary currents where strong interactions between Rossby waves, eddies, fronts and currents occur. In a future work, it will be of great interest to clearly separate these nonlinear eddies and the Rossby waves through a size classification or based on dynamical criteria as the Okubo-Weiss parameter used by *Chelton et al.* [2007].

[48] Moreover, the theoretical model from *Killworth et al.* [2004] is a simple model; strong assumptions are made. For example, the vertical chlorophyll *a* and nitrate gradients are deduced from climatologies. The statistical hypothesis from *Charria et al.* [2006] assumes that the observed ratio between CHLA and SLA can be a linear combination of the three modeled coupled processes. Furthermore, the model considers only three distinct physical/biogeochemical coupled processes; however a fourth process was described by *Dandonneau et al.* [2003], in which organic material and floating particles accumulate at the surface due to Rossby wave-induced convergence and then are misclassified as surface chlorophyll *a* concentrations by ocean color algorithms. This process, on which there is not a definite consensus [*Killworth*, 2004; *Dandonneau et al.*, 2004] can explain part of the signal observed in the South Pacific Subtropical Gyre because of the very oligotrophic conditions in this area, with very weak meridional and vertical gradients of chlorophyll *a*. In the South Atlantic Ocean, the oligotrophic gyre is not very much developed, as compared to other oceans, especially the South Pacific Ocean [*McClain et al.*, 2004], and there are strong meridional gradients of surface chlorophyll *a* concentrations, north and south of the Subtropical Gyre, as well as in the Subtropical Convergence Zone. Thus, we conclude that this fourth mechanism is unlikely to play a role in the formation of a Rossby wave signals on CHLA in the South Atlantic Ocean.

3.3. Temporal Variability of the Dominant Process: Horizontal Advection of Surface Chlorophyll *a* Concentrations

[49] In the previous section, we found that the results from the CWA are consistent with previous studies, and that when we look at the mean contributions over the 1998–2001 period the meridional advection of surface chlorophyll *a* concentrations by Rossby waves represents the dominant process, responsible of an important part of the observed signals in the chlorophyll *a* data in the South Atlantic Ocean. In this section, we take advantage of the capability of localizing the information in time, allowed by the wavelet approach, to investigate the seasonal and interannual variability of this dominant process over the South Atlantic Ocean. Therefore, we study the seasonal and interannual variability of the observed phase relationships between CHLA and SLA signals in relation with the meridional gradient of surface chlorophyll *a* concentrations deduced from the raw data of ocean color for the whole time series (from September 1997 till August 2006). The time dependent phase relationships are calculated using the CWA between the filtered signals of CHLA and SLA. The time variability of the other two processes is not investigated for two reasons. First, these two processes are not dominant over the South Atlantic Ocean. Second, we do not have databases

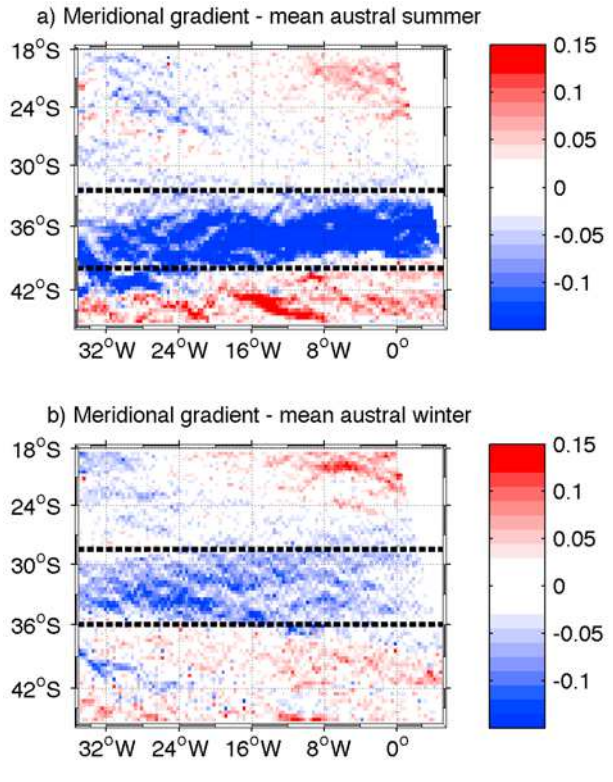

Figure 7. Meridional gradient of surface chlorophyll *a* concentrations ($\log_{10}$(mgChl.m^{-3}).degree^{-1}) from satellite observations for (a) a mean austral summer and (b) a mean austral winter. The black dashed lines represent the northern and southern limits of the strong negative meridional gradient (<−0.03 $\log_{10}$(mgChl.m^{-3}).degree^{-1}).

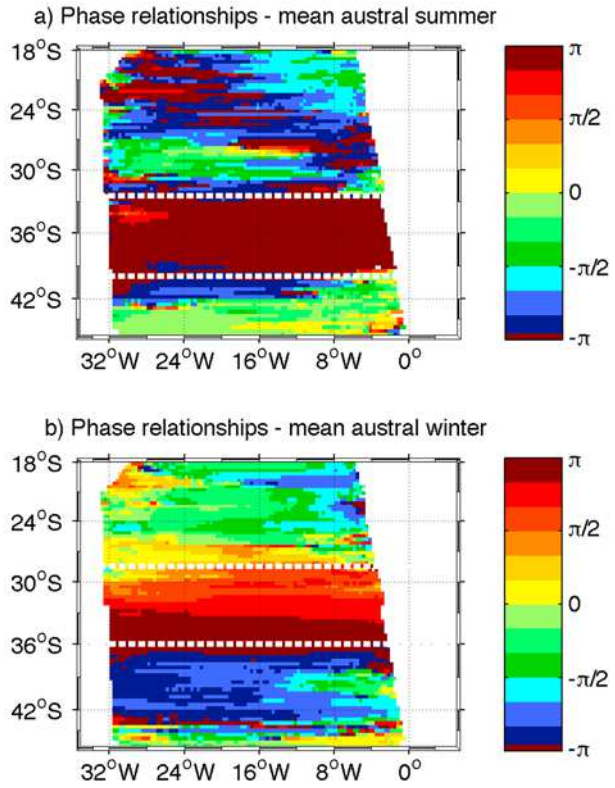

Figure 8. Phase relationships from satellite observations for (a) a mean austral summer and (b) a mean austral winter. The white dashed lines are the same limits as for Figure 7, and also represent the northern and southern limits of the area having phases mostly between $\pi/2$ and π.

over the entire South Atlantic Ocean to study the seasonal and interannual variability of the vertical gradients of chlorophyll *a* and nitrate concentrations.

3.3.1. Seasonal Variability

[50] As described by *Peterson and Stramma* [1991] and *Lass and Mohrholz* [2008], the atmospheric sea level pressure of the South Atlantic is dominated by a quasi permanent high pressure system in the subtropics which is centered near 32°S–5°W in austral summer with a maximum pressure about 1021 hPa. The maximum pressure increases in austral winter to about 1025 hPa and moves nearly 800 km toward northwest, to about 27°S–10°W. The Subtropical Atmospheric Anticyclone shifts to about 5° in latitude between austral summer and winter, with a poleward position in austral summer. As a consequence, the Trade winds and the westerlies also shift seasonally in latitude. The Intertropical Convergence Zone, region of Trade wind convergence, extends along the equator during austral summer and shifts north to about 10°N during austral winter. For the westerlies, their maximum moves poleward during austral summer.

[51] To study a potential latitudinal shift of the Subtropical Gyre and the subsequent influence on the dominant process (the meridional advection of surface chlorophyll *a* concentrations) involved with the passage of Rossby waves, the meridional gradient of surface chlorophyll *a* concentrations is examined. The meridional gradient of $\log_{10}$(chlorophyll *a* concentrations) ($\log_{10}$(mgChl.m^{-3}).degree^{-1}) is computed for each mean season. It is smoothed in latitude using a moving average over 1° to reduce the noise. Figure 7 presents the seasonal meridional gradient of surface chlorophyll *a* concentrations in austral summer (January–February–March) and winter (July–August–September). The area of negative meridional gradient is well marked in latitudinal position and intensity as compared to the area of positive meridional gradient. Therefore, we choose mainly to study the seasonal latitudinal shift for the area of negative meridional gradient for a strong negative gradient (<−0.03 $\log_{10}$(mgChl.m^{-3}).degree^{-1}; see the area between the black dashed lines on Figure 7) associated with phases between $\pi/2$ and π. During the austral summer, the meridional gradient is negative (<−0.03 $\log_{10}$(mgChl.m^{-3}).degree^{-1}) from 32.5°S to 40°S. The maximum of meridional chlorophyll *a* gradient at 37°S (not shown) characterizes the northern chlorophyll *a* front of the Subtropical Convergence Zone. In this region, *Burls and Reason* [2006] found the northern frontal feature near 36°S in the summer SST gradient using microwave satellite data. During the winter time, the area of negative meridional gradient (<−0.03 $\log_{10}$(mgChl.m^{-3}).degree^{-1}) is situated between 28.5°S and 36°S (seasonal shift of 4°) with a maximum at 33.5°S (northern chlorophyll *a* front; not shown). The northern chlorophyll *a* front moves equatorward from about 3.5° and becomes less intense between the austral summer and winter. These observations are in agreement with *Burls and Reason* [2006] who argued for noticeable seasonal changes in frontal intensity and a small

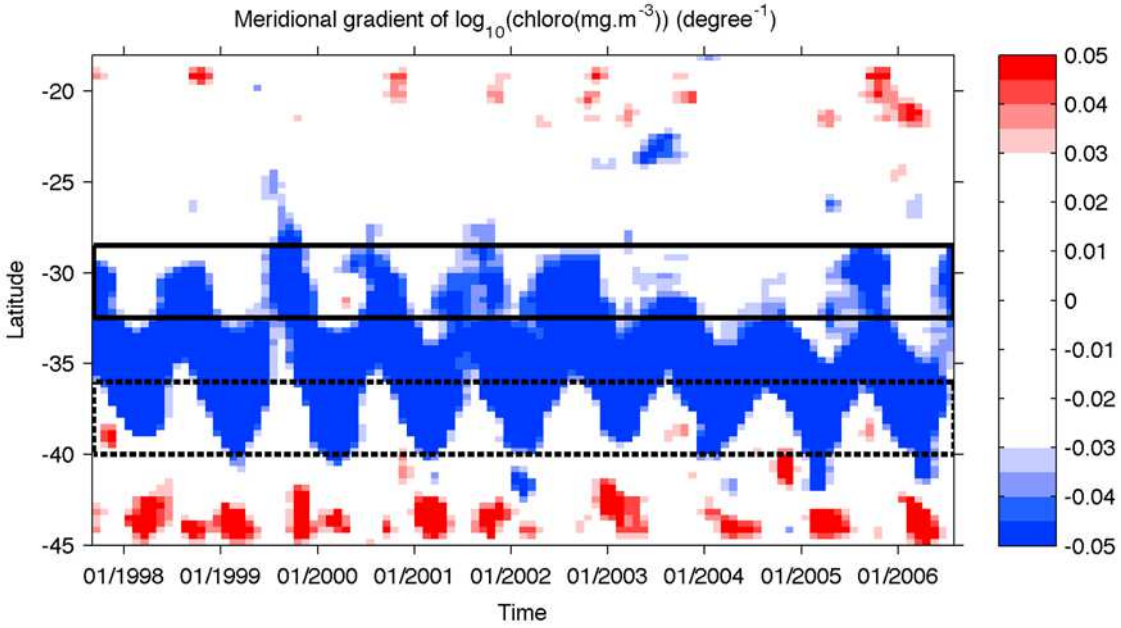

Figure 9. Latitude/time diagram of the meridional chlorophyll *a* gradient ($\log_{10}$(mgChl.m^{-3}).degree^{-1}) from satellite observations. The black solid (dashed) rectangle represents the area situated between the mean winter and summer limits of the northern (southern) limit of the strong negative chlorophyll *a* gradient.

seasonal shift in the Northern Subtropical Front in SST related to the seasonal shift of the Subtropical Atmospheric Anticyclone [*Peterson and Stramma*, 1991; *Lass and Mohrholz*, 2008].

[52] With the same methodology, Figure 8 presents the seasonal phase relationships in austral summer and winter. As mentioned in the previous paragraph, we focus on the area of strong negative meridional gradient (phase relationships between $\pi/2$ and π according to the theoretical model). In section 3.2.1, the phase relationships from 1998 to 2001 show that between 30°S and 39°S, observed phases are mainly between $\pi/2$ and π (or around $-\pi$) (Figure 5a). Here, this phase range shifts 4° degrees in latitude between austral summer (from 32.5°S to 40°S) and winter (from 28.5°S to 36°S), in agreement with the seasonal displacement of the negative meridional chlorophyll *a* gradient (<−0.03 $\log_{10}$(mgChl.m−^{3}).degree−^{1}). So, this seasonal variability of the phase relationships is shown with the

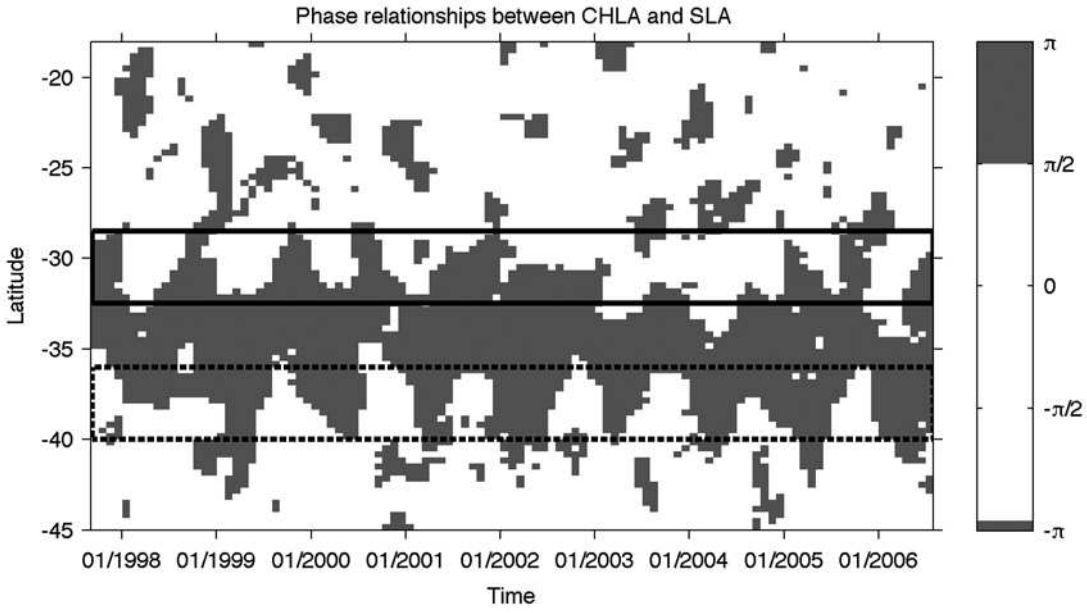

Figure 10. Latitude/time diagram of the phase relationships between CHLA and SLA from satellite observations. The same rectangles as in Figure 9 are plotted.

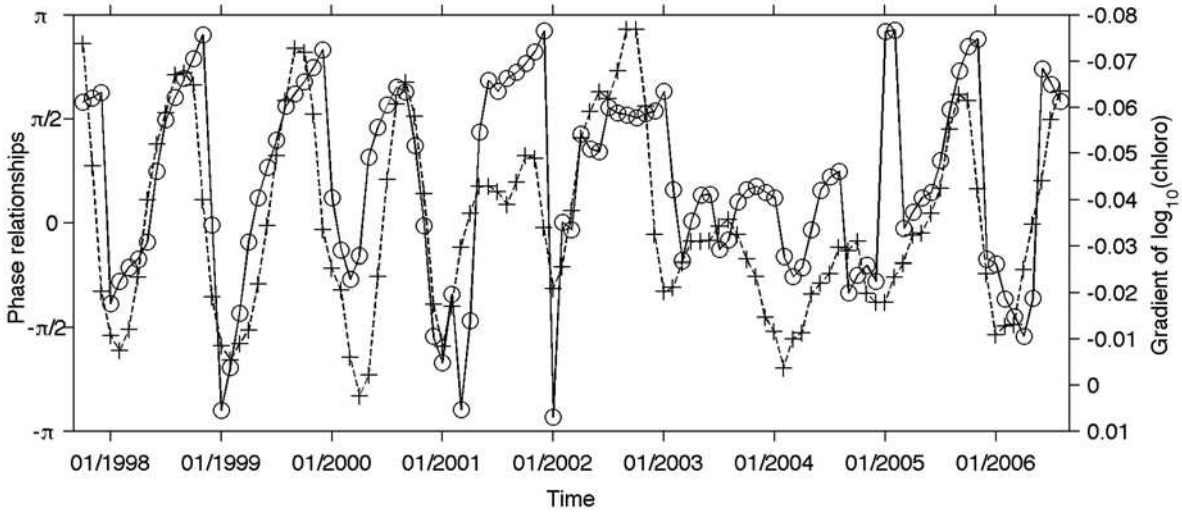

Figure 11. Temporal evolution of the mean meridional chlorophyll *a* gradient ($\log_{10}$(mgChl.m^{-3}).degree^{-1}) (dashed line with crosses, axis to the right) and the mean phase relationships between CHLA and SLA (solid line with circles, axis to the left) for latitudes located between 30°S and 31°S. The meridional chlorophyll *a* gradient is plotted with a reverse axis for ease of comparison.

meridional shift (4°) of the horizontal chlorophyll *a* gradient of the Subtropical Convergence Zone, related to the seasonal shift of the Subtropical Atmospheric Anticyclone [*Peterson and Stramma*, 1991; *Burls and Reason*, 2006; *Lass and Mohrholz*, 2008]. This seasonal meridional variability of the associated coupled processes may have an influence on the biological production via the latitudinal variation of the available light and nutrient fields.

3.3.2. Interannual Variability

[53] The interannual variability of the meridional chlorophyll *a* gradient and the phase relationships observed between the CHLA and SLA signals are now investigated. Figure 9 presents a time/latitude diagram of the meridional chlorophyll *a* gradient. The gradient is averaged in longitude and smoothed in time and latitude (moving average over 3 months and over 5/3°). The interannual study requires a heavier smoothing than the seasonal study to reduce the noise and observe the trends, as the interannual signal is weaker. Here, the same comment as for the seasonal variability can be made. The area of strong negative meridional gradient is very developed and, the positive gradients are weaker. So, we study the interannual variability of the negative meridional gradient, with the same threshold: we follow the gradients less than -0.03 $\log_{10}$(mgChl.m^{-3}).degree^{-1} (regions in blue on Figure 9) associated with phases between $\pi/2$ and π.

[54] First, we focus on the northern limit of the strong negative gradient (<-0.03 $\log_{10}$(mgChl.m^{-3}).degree^{-1}). This limit is located near 30°S–31°S and shifts around 4° in latitude as a function of the season (~28.5°S during winter and ~32.5°S during summer; see the black solid rectangle on Figure 9). For specific years, this seasonal cycle is perturbed. The years 1999, 2003, and 2004 can be emphasized. Indeed, the strong negative meridional chlorophyll *a* gradient moves equatorward up to 25°S during the 1999 winter. On the other hand, in 2003 and 2004 it hardly migrates equatorward at all, and stays around 31°S. To observe a potential impact on the phase relationships (or phase differences) between CHLA and SLA (Figure 10), the same methodology is used. In 2003 and 2004 the area with phase range between $\pi/2$ and π (or around $-\pi$) does not migrate equatorward up to 27°S–28°S during the winter season and remain at 31°S as well as the strong negative meridional chlorophyll *a* gradient (Figure 9). Always focusing on the northern limit of the area with phases between $\pi/2$ and π, the winter 1999 does not present any anomaly whereas the negative meridional chlorophyll *a* gradient moves exceptionally equatorward. In this case, the observed phase relationships do not represent any of the theoretical mechanisms, because they should be situated between $\pi/2$ and π until 25°S (see section 2.3.1) using the theoretical process model from *Killworth et al.* [2004]. In 1998, the area with phases between $\pi/2$ and π extends farther equatorward, and this particularity is not observed in the meridional chlorophyll *a* gradient. Other contributions (vertical mechanisms) could explain this difference between the meridional chlorophyll *a* gradient and the phase relationships in 1998, as the phase relationships are situated between $\pi/2$ and π for both theoretical vertical mechanisms (see section 2.3.1).

[55] Figure 11 presents the mean meridional chlorophyll *a* gradient (dashed line with crosses) and the mean phase relationships between CHLA and SLA (solid line with circles) for latitudes located between 30°S and 31°S (mean position of the limit between the oligotrophic gyre and the area with a strong negative gradient; see Figure 9), using the same methodology as for Figures 9 and 10. The meridional chlorophyll *a* gradient presents a clear seasonal cycle during the whole time series, although its amplitude is reduced in 2003 and 2004. The gradient is strongly negative during the austral winter season, and it is weakly negative (close to zero) during the austral summer season. From September 1997 to the end of 2002 and from 2005 to August 2006, the meridional chlorophyll *a* gradient and the phase relationships are well correlated (correlation coefficient

around −0.65). Phases are positive during the austral winter and negative during austral summer. The situations described for 1998 and 1999 in the previous paragraph do not appear on Figure 11 as we focus on latitudes 30–31°S, these situations are located closer to the equator. Between 30°S and 31°S, we can deduce that the process of meridional advection of surface chlorophyll *a* concentrations associated with the meridional chlorophyll *a* gradient is likely to explain an important part of the signal observed on the phase relationships from September 1997 to the end of 2002 and from 2005 to August 2006. In 2003 and 2004, the situation is different. The phase relationships do not follow the seasonal cycle of the meridional gradient (correlation coefficient < −0.12) described for the other years. The phase relationships between CHLA and SLA stay close to zero both years as the seasonal variability of the meridional gradient is reduced with weak value in winter (>−0.035 and >−0.03 $\log_{10}(\text{mgChl.m}^{-3}).\text{degree}^{-1}$ in 2003 and 2004, respectively). The usual seasonal cycle for both data sets is situated poleward, south of 31°S–32°S in 2003 and 2004 (see Figures 9 and 10). Between 30°S and 31°S, the meridional advection process of surface chlorophyll *a* concentrations does not seem to play the predominant role in the chlorophyll *a* signature of Rossby waves in 2003 and 2004. This result illustrates that, while generally the dominant mechanism is horizontal advection (as shown by *Killworth et al.* [2004]), other processes cannot be ruled out as they must still play a significant role in specific places at specific times.

[56] The same pattern can also be observed but weaker at the southern limit of the strong negative meridional chlorophyll *a* gradient (<−0.03 $\log_{10}(\text{mgChl.m}^{-3}).\text{degree}^{-1}$) (Figure 9). This transition is situated near 40°S during the austral summer, while it is usually close to 36°S in the austral winter (see the black dashed rectangle on Figure 9). The Subtropical Convergence Zone, with important seasonal modifications and mesoscale activity, is a highly variable region. However, some interannual variability can be highlighted. During the summer season, this transition does not go poleward of 39°S for 1998 and 2003 as compared to the other years (around 40°S). This specificity can also be observed in austral summer 1998 on the phase relationships (Figure 10). The area with phases range between $\pi/2$ and π (or around $-\pi$) does not go poleward of 38°S. The same representation as Figure 11 is not shown for the southern limit as the interannual variability is weaker.

[57] *Burls and Reason* [2006] also observed interannual variability in the SST gradients using microwave satellite data in the South Atlantic Ocean. For example, in winter a broad region of relatively enhanced gradient in the 36°S–40°S zone for 2003 and 2004 could correspond to the Southern Subtropical Front. They studied the associated large scale atmospheric circulation with the NCEP/NCAR reanalysis over the midlatitude South Atlantic and found July 2002 rather different from July 2003 and 2004. In the latter two years, the South Atlantic Anticyclone is stronger and shifted toward the south. The enhanced and southward shifted anticyclone in July 2004 is also found in the QuickSCAT surface winds. This anticyclone center is shifted poleward up to 35°S as compared to near 30°S in July 2003 and about 27°S in 2002. The permanent high pressure system is usually centered near 27°S in austral winter [*Peterson and Stramma*, 1991; *Lass and Mohrholz*, 2008]. *Burls and Reason* [2006] concluded that the SST gradients between about 33°S and 43°S in the South Atlantic Ocean seem to be related to Ekman convergence and their interannual variability linked to that in the observed winds. These results are quite in agreement with the poleward position of the meridional chlorophyll *a* gradient and phase relationships between CHLA and SLA for both years 2003 and 2004 that we have described above.

[58] *Grodsky and Carton* [2006] considered the implications of the tropical/extratropical connection for the climate of the South Atlantic through the relationship between interannual sea level and SST between October 1992 and June 2005. They observed higher leading sea level (decomposed into EOFs, Empirical Orthogonal Functions) than average in 1998, 1999, 2003, and 2004 in good agreement with negative anomalies of a climatic index: the St Helena Island climatic index (HIX) developed by *Feistel et al.* [2003]. HIX is the time series of the leading EOF of pressure, temperature and precipitation at the St Helena weather station record. The same correlation was found for the time series of the leading EOF of SST. These in-phase relationships between SST and sea level in the tropics extend into the southeastern subtropics. In contrast, SST in the southwestern subtropics varies out of phase with SST in the southern Gulf of Guinea, giving rise to a northeast/southwest SST dipole in conjunction with a weakening of the southeasterly Trade winds and development of a more intense southern subtropical high pressure. The study of *Grodsky and Carton* [2006] suggests a connection between the tropics and the subtropics for the interannual variability of the South Atlantic Ocean, and confirms the findings by *Burls and Reason* [2006] for an enhanced and poleward shift of the atmospheric South Atlantic Anticyclone for the winter season of 2003 and 2004. Further research is needed to clarify this possible link between the tropics and the subtropics and its influence on interannual variability of meridional SST and chlorophyll *a* gradients between 18°S and 45°S in the South Atlantic Ocean.

4. Conclusions and Perspectives

[59] To conclude, this paper highlights the relative importance of three processes explaining the Rossby wave signature in ocean color in the South Atlantic Ocean. Three distinct subdomains are distinguished in this basin. North of the Subtropical Gyre northern boundary, the meridional advection of surface chlorophyll *a* concentrations contributes for 63.2%, the upwelling of nitrates for 33.5%, and the uplifting of chlorophyll *a* for 3.3%. Between the northern boundary of the Subtropical Gyre and 39°S, a mean contribution of 48.5% is attributed to the horizontal advection, 20.5% to the uplifting of chlorophyll *a* and, 31% to the upwelling of nitrates. South of 39°S, the horizontal process explains 58.8% of the observed signal, uplifting of chlorophyll *a* 9.7%, and upwelling of nitrates 31.5%. The meridional advection of surface chlorophyll *a* concentrations represents the dominant process in the South Atlantic Ocean. The present work also investigates seasonal and interannual variations of this dominant process. The temporal variability of the phase relationships between CHLA and SLA with the meridional gradient of chlorophyll *a* concentrations is analyzed. A clear seasonal cycle shows a meridional shift in

latitude of both data sets. For the interannual variability, specific years (2003 and 2004) are observed at 30°S, where the meridional gradient of chlorophyll *a* concentrations and the phase relationships do not follow the usual seasonal cycle. This seasonal and interannual variability can be associated with the variability of the South Atlantic Anticyclone [*Burls and Reason*, 2006; *Grodsky and Carton*, 2006].

[60] To complete the study of temporal variations, more knowledge about the vertical gradients are needed, such as an interannual data set of vertical gradients of chlorophyll *a* and nutrient concentrations. Longer SLA and ocean color data records are required to really quantify the interannual variability of the phase relationships of both data sets and its possible link with the tropical connections (ENSO) [e.g., *Grodsky and Carton*, 2006] and/or extratropical connections (SAM) [e.g., *Pottier et al.*, 2004]. The seasonal and interannual variation of the relative contribution of all the different processes (i.e., including the vertical ones) is not studied here. To do so, the theoretical model of the different processes would have to be transformed into a coupled model capable to evolve with time.

[61] **Acknowledgments.** The CNES and Midi-Pyrénées Region are thanked for the financial Ph.D. support attributed to E. Gutknecht. We would like to thank the CNES support attributed to I. Dadou and V. Garçon and the Marie Curie support (MEIF-CT-2006-039180) attributed to G. Charria as an IntraEuropean postdoctoral fellowship. The Sea Level Anomaly data from the DUACS processing were developed by AVISO. Ocean color data were produced by the SeaWiFS project at GSFC and obtained from the DAAC. We thank J. Sudre (LEGOS) for extracting the SeaWiFS data. Wavelet software was provided by C. Torrence and G. P. Compo, and is available at http://paos.colorado.edu/research/wavelets/. We express our special thanks to M. Thomas (University of East Anglia, UK) who provided us with simulation outputs including both eddies and Rossby waves, and allowed us to confirm that our filtering procedure can be applied to real data with confidence.

References

Burls, N. J., and C. J. C. Reason (2006), Sea surface temperature fronts in the midlatitude South Atlantic revealed by using microwave satellite data, *J. Geophys. Res.*, *111*, C08001, doi:10.1029/2005JC003133.

Campbell, J. W. (1995), The lognormal distribution as a model for bio-optical variability in the sea, *J. Geophys. Res.*, *100*(C7), 13,237–13,254, doi:10.1029/95JC00458.

Challenor, P. G., P. Cipollini, and D. Cromwell (2001), Use of the 3D Radon transform to examine the properties of oceanic Rossby waves, *J. Atmos. Oceanic Technol.*, *18*(9), 1558–1566. (Corrigendum, *J. Atmos. Oceanic Technol.*, 19(5), 828, 2002.)

Charria, G., F. Mélin, I. Dadou, M.-H. Radenac, and V. Garçon (2003), Rossby wave and ocean color: The cells uplifting hypothesis in the South Atlantic Subtropical Convergence Zone, *Geophys. Res. Lett.*, *30*(3), 1125, doi:10.1029/2002GL016390.

Charria, G., I. Dadou, P. Cipollini, M. Drévillon, P. De Mey, and V. Garçon (2006), Understanding the influence of Rossby waves on surface chlorophyll *a* concentrations in the North Atlantic Ocean, *J. Mar. Res.*, *64*(1), 43–71, doi:10.1357/002224006776412340.

Charria, G., I. Dadou, P. Cipollini, M. Drévillon, and V. Garçon (2008), Influence of Rossby waves on primary production from a coupled physical-biogeochemical model in the North Atlantic Ocean, *Ocean Sci.*, *4*(3), 199–213.

Chelton, D. B., and M. G. Schlax (1996), Global observations of oceanic Rossby waves, *Science*, *272*, 234–238, doi:10.1126/science.272.5259.234.

Chelton, D. B., M. G. Schlax, R. M. Samelson, and R. A. de Szoeke (2007), Global observations of large oceanic eddies, *Geophys. Res. Lett.*, *34*, L15606, doi:10.1029/2007GL030812.

Cipollini, P., D. Cromwell, P. G. Challenor, and S. Raffaglio (2001), Rossby waves detected in global ocean colour data, *Geophys. Res. Lett.*, *28*(2), 323–326, doi:10.1029/1999GL011231.

Cipollini, P., G. D. Quartly, P. G. Challenor, D. Cromwell, and I. S. Robinson (2006), Remote sensing of extra-equatorial planetary waves, in *Manual of Remote Sensing*, vol. 6, *Remote Sensing of the Marine Environment*, edited by J. F. R. Gower, chap. 3, pp. 61–84, Am. Soc. for Photogramm. and Remote Sens., Bethesda, Md.

Colberg, F., C. J. C. Reason, and K. Rodgers (2004), South Atlantic response to El Niño-Southern Oscillation induced climate variability in an ocean general circulation model, *J. Geophys. Res.*, *109*, C12015, doi:10.1029/2004JC002301.

Conkright, M. E., T. O'Brien, S. Levitus, T. P. Boyer, J. Antonov, and C. Stephens (1998), *World Ocean Atlas 1998*, vol. 10, *Nutrients and Chlorophyll of the Atlantic Ocean, NOAA Atlas NESDIS*, vol. 36, 245 pp., NOAA, Silver Spring, Md.

Dandonneau, Y., A. Vega, H. Loisel, Y. Du Penhoat, and C. Menkes (2003), Oceanic Rossby waves acting as a "Hay Rake" for ecosystem floating by-products, *Science*, *302*(5650), 1548–1551, doi:10.1126/science.1090729.

Dandonneau, Y., C. Menkes, T. Gorgues, and G. Madec (2004), Response to comment on "Oceanic Rossby waves acting as a 'Hay Rake' for ecosystem floating by-products," *Science*, *304*(5669), 390, doi:10.1126/science.1095997.

Deans, S. R. (1983), *The Radon Transform and Some of its Applications*, Wiley-Interscience, New York.

Feistel, R., E. Hagen, and K. Grant (2003), Climatic changes in the subtropical Southeast Atlantic: The St Helena island climate index (1893–1999), *Prog. Oceanogr.*, *59*, 321–337, doi:10.1016/j.pocean.2003.07.002.

Fu, L. L., and D. B. Chelton (2001), Large-scale ocean circulation, in *Satellite Altimetry and Earth Sciences*, edited by L. L. Fu and A. Cazenave, pp. 133–169, Academic, San Diego, Calif.

Grodsky, S. A., and J. A. Carton (2006), Influence of the tropics on the climate of the South Atlantic, *Geophys. Res. Lett.*, *33*, L06719, doi:10.1029/2005GL025153.

Haarsma, R. J., E. J. D. Campos, and F. Molteni (2003), Atmospheric response to South Atlantic SST dipole, *Geophys. Res. Lett.*, *30*(16), 1864, doi:10.1029/2003GL017829.

Handoh, I. C., G. R. Bigg, A. J. Matthews, and D. P. Stevens (2006), Interannual variability of the Tropical Atlantic independent of and associated with ENSO: Part II. The South Tropical Atlantic, *Int. J. Climatol.*, *26*, 1957–1976, doi:10.1002/joc.1342.

Hughes, C. W. (1995), Rossby waves in the Southern Ocean: A comparison of TOPEX/POSEIDON altimetry with model predictions, *J. Geophys. Res.*, *100*(C8), 15,933–15,950, doi:10.1029/95JC01380.

Killworth, P. D. (2004), Comment on "Oceanic Rossby waves acting as a 'Hay Rake' for ecosystem floating by-products," *Science*, *304*(5669), 390, doi:10.1126/science.1094870.

Killworth, P. D., and J. R. Blundell (2003a), Long extratropical planetary wave propagation in the presence of slowly varying mean flow and bottom topography. Part I: The local problem, *J. Phys. Oceanogr.*, *33*(4), 784–801, doi:10.1175/1520-0485(2003)33<784:LEPWPI>2.0.CO;2.

Killworth, P. D., and J. R. Blundell (2003b), Long extratropical planetary wave propagation in the presence of slowly varying mean flow and bottom topography. Part II: Ray propagation and comparison with observations, *J. Phys. Oceanogr.*, *33*(4), 802–821, doi:10.1175/1520-0485(2003)33<802:LEPWPI>2.0.CO;2.

Killworth, P. D., P. Cipollini, B. M. Uz, and J. R. Blundell (2004), Physical and biological mechanisms for planetary waves observed in satellite-derived chlorophyll, *J. Geophys. Res.*, *109*, C07002, doi:10.1029/2003JC001768.

Kumar, P., and E. Foufoula-Georgiou (1994), Wavelet analysis in geophysics: An introduction, in *Wavelets in Geophysics*, edited by E. Foufoula-Georgiou and P. Kumar, pp. 1–43, Academic, San Diego, Calif.

Lass, H. U., and V. Mohrholz (2008), On the interaction between the subtropical gyre and the Subtropical Cell on the shelf of the SE Atlantic, *J. Mar. Syst.*, *74*(1–2), 1–43, doi:10.1016/j.jmarsys.2007.09.008.

Le Traon, P. Y., F. Nadal, and N. Ducet (1998), An improved mapping method of multisatellite altimeter data, *J. Atmos. Oceanic Technol.*, *15*(2), 522–534, doi:10.1175/1520-0426(1998)015<0522:AIMMOM>2.0.CO;2.

Longhurst, A. (1998), *Ecological Geography of the Sea*, 398 pp., Academic, San Diego, Calif.

Louanchi, F., and R. G. Najjar (2001), Annual cycles of nutrients and oxygen in the upper layers of the North Atlantic Ocean, *Deep Sea Res. Part II*, *48*(10), 2155–2171, doi:10.1016/S0967-0645(00)00185-5.

Machu, E., B. Ferret, and V. Garçon (1999), Phytoplankton pigment distribution from SeaWiFS data in the Subtropical Convergence Zone south of Africa: A wavelet analysis, *Geophys. Res. Lett.*, *26*(10), 1469–1472, doi:10.1029/1999GL900256.

Maharaj, A. M., P. Cipollini, and N. J. Holbrook (2005), Observed variability of the South Pacific westward sea level anomaly signal in the presence of bottom topography, *Geophys. Res. Lett.*, *32*, L04611, doi:10.1029/2004GL020966.

Matano, R. P., and E. J. Beier (2003), A kinematic analysis of the Indian/Atlantic interocean exchange, *Deep Sea Res. Part II*, *50*(1), 229–249, doi:10.1016/S0967-0645(02)00395-8.

McClain, C. R., M. L. Cleave, G. C. Feldman, W. W. Gregg, S. B. Hooker, and N. Kuring (1998), Science quality SeaWiFS data for global biosphere research, *Sea Technol.*, *39*(9), 10–16.

McClain, C. R., S. R. Signorini, and J. R. Christian (2004), Subtropical gyre variability observed by ocean-color satellites, *Deep Sea Res. Part II*, *51*(1–3), 281–301, doi:10.1016/j.dsr2.2003.08.002.

O'Reilly, J. E., S. Maritorena, B. G. Mitchell, D. A. Siegel, K. L. Carder, S. A. Garver, M. Kahru, and C. R. McClain (1998), Ocean color chlorophyll algorithms for SeaWiFS, *J. Geophys. Res.*, *103*(C11), 24,937–24,953, doi:10.1029/98JC02160.

Peterson, R. G., and L. Stramma (1991), Upper-level circulation in the South Atlantic Ocean, *Prog. Oceanogr.*, *26*(1), 1–73, doi:10.1016/0079-6611(91)90006-8.

Pierini, S. (2005), A model study of the spectral structure of boundary-driven Rossby waves and related altimetric implications, *J. Phys. Oceanogr.*, *35*(2), 218–231, doi:10.1175/JPO-2680.1.

Pierini, S. (2006), Seasonal and interannual variability of the North Pacific Ocean: Modeling results and their validation through altimeter data, paper presented at 15 Years of Progress in Radar Altimetry Symposium, Eur. Space Agency, Cent. Natl. d'Étud. Spatiales, Venice, Italy, 13–18 Mar.

Polito, P. S., and W. T. Liu (2003), Global characterization of Rossby waves at several spectral bands, *J. Geophys. Res.*, *108*(C1), 3018, doi:10.1029/2000JC000607.

Pottier, C., J.-P. Céron, J. Sudre, I. Dadou, S. Belamari, and V. Garçon (2004), Dominant propagating signals in sea level anomalies in the Southern Ocean, *Geophys. Res. Lett.*, *31*, L11305, doi:10.1029/2004GL019565.

Pottier, C., V. Garçon, G. Larnicol, J. Sudre, P. Schaeffer, and P. Y. Le Traon (2006), Merging SeaWiFS and MODIS-Aqua ocean color data in North and Equatorial Atlantic using weighted averaging and objective analysis, *IEEE Trans. Geosci. Remote Sens.*, *44*(11), 3436–3451, doi:10.1109/TGRS.2006.878441.

Quartly, G. D., P. Cipollini, D. Cromwell, and P. G. Challenor (2003), Rossby waves: Synergy in action, *Philos. Trans. R. Soc. London Ser. A*, *361*(1802), 57–63, doi:10.1098/rsta.2002.1108.

Reason, C. J. C., L. A. Mysak, and P. F. Cummins (1987), Generation of annual-period Rossby waves in the South Atlantic Ocean by the wind stress curl, *J. Phys. Oceanogr.*, *17*(11), 2030–2042, doi:10.1175/1520-0485(1987)017<2030:GOAPRW>2.0.CO;2.

Rio, M. H., P. Schaeffer, F. Hernandez, and J. M. Lemoine (2005), The estimation of the ocean Mean Dynamic Topography through the combination of altimetric data, in-situ measurements and GRACE geoid: From global to regional studies, paper presented at Geoid and Ocean Circulation in the North Atlantic International Workshop, Eur. Comm., Luxembourg, 13–15 Apr.

Robertson, A. W., J. D. Farrara, and C. R. Mechoso (2003), Simulations of the atmospheric response to South Atlantic sea surface temperature anomalies, *J. Clim.*, *16*(15), 2540–2551, doi:10.1175/1520-0442(2003)016<2540:SOTART>2.0.CO;2.

Schopf, P. (1981), Beta-dispersion of low-frequency Rossby waves, *Dyn. Atmos. Oceans*, *5*(3), 187–214, doi:10.1016/0377-0265(81)90011-7.

Siegel, D. A. (2001), The Rossby rototiller, *Nature*, *409*(6820), 576–577, doi:10.1038/35054659.

Sterl, A., and W. Hazeleger (2003), Coupled variability and air-sea interaction in the South Atlantic Ocean, *Clim. Dyn.*, *21*(7–8), 559–571, doi:10.1007/s00382-003-0348-y.

Torrence, C., and G. P. Compo (1998), A practical guide to wavelet analysis, *Bull. Am. Meteorol. Soc.*, *79*(1), 61–78, doi:10.1175/1520-0477(1998)079<0061:APGTWA>2.0.CO;2.

Torrence, C., and P. J. Webster (1999), Interdecadal changes in the ENSO-Monsoon System, *J. Clim.*, *12*, 2679–2690, doi:10.1175/1520-0442(1999)012<2679:ICITEM>2.0.CO;2.

Uz, B. M., J. A. Yoder, and V. Osychny (2001), Pumping of nutrients to ocean surface waters by the action of propagating planetary waves, *Nature*, *409*(6820), 597–600, doi:10.1038/35054527.

Venegas, S. A., L. A. Mysak, and D. N. Straub (1997), Atmosphere-ocean coupled variability in the South Atlantic, *J. Clim.*, *10*(11), 2904–2920, doi:10.1175/1520-0442(1997)010<2904:AOCVIT>2.0.CO;2.

G. Charria and P. Cipollini, National Oceanography Centre, European Way, Southampton SO14 3ZH, UK.

I. Dadou, V. Garçon, and E. Gutknecht, Laboratoire d'Etudes en Géophysique et Océanographie Spatiales, UMR 5566, 14 Ave. Edouard Belin, UPS, CNES, CNRS, IRD, F-31400 Toulouse, France. (isabelle.dadou@legos.obs-mip.fr)